

# Metastable optical gratings in compound semiconductors

D. D. Nolte

Department of Physics, Purdue University, West Lafayette, Indiana 47907-1396

(Received 8 February 1996; accepted for publication 14 February 1996)

Spatially nonuniform optical illumination of semiconductors containing metastable defects, such as GaAs:EL2 and DX-related defects in III–V and II–VI semiconductors, induces metastable photorefractive and free-carrier gratings. Detailed calculations of the space-charge gratings in these materials are made as functions of fringe spacing and optical exposure. In both defect cases a unique *nonequilibrium* Fermi level, obtained from a charge balance approximation, can be defined that describes the spatial charge transfer and the resulting modulation of the optical properties of the semiconductor, without resorting to multiple quasi-Fermi levels. The process of writing holographic gratings with low intensities is analogous to adiabatic modulation doping. The transfer of charge from photoquenched regions to nonphotoquenched regions determines the highest spatial resolution that can be supported in the materials. In the case of EL2, the modulation doping produces a *p-i-p-i* doped superlattice. The DX defects support smaller Fermi level modulation, but have larger optical effects based on persistent photoconductivity and free-carrier gratings. © 1996 American Institute of Physics. [S0021-8979(96)09710-4]

## I. INTRODUCTION

Volumetric optical data storage applications require nonlinear optical materials in which optical information can be stored semipermanently, and then reversibly erased. Multiple read-and-write memory materials, such as magnetic materials used in magnetic recording, rely on reversible transformations from one metastable state to another. In semiconductors, the most notable metastable states are metastable defects. The most thoroughly studied metastable defects are the so-called EL2 defect in GaAs (Ref. 1) and the DX family of defects in III–V and II–VI alloys.<sup>2</sup> These defects can be transformed into metastable states by optical excitation at low temperature, and can recover by thermal regeneration. The optical sensitivity of these defects, and the strong optical gratings that are produced, make them candidates for optical information recording.

The first use of metastable defects to write volume optical holograms in semiconductors utilized GaAs:EL2.<sup>3</sup> Semipermanent holographic gratings were written in semi-insulating liquid-encapsulated Czochralski GaAs at temperatures below 140 K using 1.06  $\mu\text{m}$  laser radiation. An optical signal diffracted from the gratings was shown to have a diffracted intensity more than an order of magnitude larger than the traditional photorefractive diffraction efficiency for the same temperature.<sup>3</sup> This large diffraction efficiency was attributed to quasiequilibrium Fermi-level modulation, during which the EL2 defects were optically quenched within the bright fringes of the hologram, but were left unaffected in the dark fringes. The liberation of holes during the quenching process produces a *p-i-p-i* doping superlattice.<sup>4</sup> The band bending of the superlattice generated strong electro-optic gratings, with grating amplitudes much larger than possible by thermal diffusion alone. These gratings were shown to be semipermanent, and could be read nondestructively by laser radiation at 1.32  $\mu\text{m}$  wavelength.<sup>4</sup> Further studies of GaAs:EL2 focused on the role of charge transfer and the generation of nonlocal index changes,<sup>5</sup> as well as processes

that limited the magnitude of the gratings relative to the theoretical maximum grating amplitudes.<sup>6</sup>

Studies of optically induced metastable gratings in DX-related materials were reported with even larger index changes and diffraction efficiencies than observed in the GaAs:EL2 system.<sup>7</sup> The large index gratings in these materials were attributed to free-carrier gratings from carriers liberated from the high concentration of DX donors in the bright fringes.<sup>8</sup> The index gratings in this material were shown to respond locally to the illumination,<sup>9</sup> illustrating an important difference between the grating formation mechanisms in the EL2 and DX systems. The spatial resolution of the DX-related gratings were also shown to be extremely high,<sup>8</sup> but finite.

In this article, we present a coherent theoretical description of metastable grating formation that applies for both the EL2 and DX systems. The underlying principle for both systems is optically induced Fermi-level modulation, in which the gratings are viewed as modulation-doped superlattices in thermal equilibrium with stable defect states. The superlattices are assumed to be generated adiabatically, with slow incremental exposure. This approach yields accurate descriptions of the induced optical gratings, including quantitative values for grating amplitudes and limiting grating periods. In Sec. II we present the fundamentals of induced gratings followed by a description of the compensation mechanisms of the EL2 and DX defects in Sec. III. The theoretical treatment is described in Sec. IV, and applied to the EL2 and DX defects in Secs. V and VI. Unresolved theoretical issues are discussed in Sec. VII, with suggestions of theoretical extensions to the theory presented here, especially for conditions of nonadiabatic grating formation.

## II. OPTICAL GRATINGS

The simplest holographic gratings are the sinusoidal interference fringes caused by two overlapping coherent light fields. The intensity as a function of position is given by

$$I(x) = I_0(1 + m \cos Kx), \quad (1)$$

where  $m$  is the contrast ratio of the fringes. A modulation index  $m=0.9$  is used in all the simulations presented in this article. The spatially varying light intensity induces changes in the optical properties of nonlinear optical materials. Within the class of photorefractive and related materials, there are three mechanisms that produce optical gratings: the electro-optic effect, induced absorption, and free-carrier gratings.

### A. Electro-optic gratings

Electric fields change the refractive index of noncentrosymmetric crystals through linear electro-optic effects. During photorefractive experiments on semiconductor crystals without applied electric fields, internal space-charge fields are generated by diffusion of photocarriers. The amplitude of the diffusion field is<sup>10</sup>

$$E_D = 2\pi \frac{k_B T}{e \Lambda}, \quad (2)$$

where  $\Lambda$  is the fringe spacing of the holographic grating. When the space-charge electric field is oriented along a  $\langle 100 \rangle$  axis of the crystal, and a light wave travels along an orthogonal  $\langle 110 \rangle$  axis with a polarization perpendicular to the field, the wave experiences a change in the refractive index given by

$$\Delta n = -\frac{1}{2} n^3 r_{41} E, \quad (3)$$

where  $r_{41}$  is the electro-optic coefficient and  $E$  is the electric field. This crystal geometry is called the ‘‘holographic cut’’ and is commonly used as the crystal orientation for studies of photorefractive semiconductors. In GaAs  $r_{41} = 1$  pm/V. For a fringe spacing of  $1 \mu\text{m}$  at room temperature the electric field is  $E_D = 1.6$  kV/cm, and the change in the refractive index is therefore  $\Delta n = 4 \times 10^{-6}$ .

### B. Absorption gratings

Optical illumination commonly changes defect occupancy by photoionization and trapping. Defects can be partially emptied or filled during illumination depending on optical and capture cross sections. The changes in the defect occupancy produce changes in the optical absorption of the crystal, described as induced absorption or induced bleaching with positive or negative  $\Delta\alpha$ . The total absorption change in response to changes in defect occupancies  $\Delta N^q$  of the  $q$ th charge states is

$$\Delta\alpha(\omega; x) = \sum_q [s_e^q(\omega) - s_h^q(\omega)] \Delta N^q [I(x)], \quad (4)$$

where  $s_{e,h}$  are the electron and hole optical cross sections. When the optical illumination is spatially nonuniform, as during holographic writing, absorption gratings of spatial frequency  $K$  with Fourier amplitudes  $\Delta\alpha_K$  are formed.

### C. Free-carrier gratings

The complex dielectric response of a semiconductor is a function of free carrier density. The simplest model for the

contribution of the free carriers to the dielectric function is the Drude model.<sup>11</sup> The dielectric function of a plasma with a density of  $N$  charge carriers is

$$\epsilon(\omega) = \epsilon(\infty) - \frac{\tilde{\omega}_p^2}{\omega^2} + i\gamma \frac{\tilde{\omega}_p^2}{\omega^3}, \quad (5)$$

where

$$\tilde{\omega} = \frac{Ne^2}{\epsilon_0 \epsilon(\infty) m^*} \quad (6)$$

is the plasma frequency  $m^*$  is the free carrier effective mass,  $\epsilon(\infty)$  is the frequency-dependent background dielectric function, and  $\gamma$  is the free-carrier scattering rate. When a change in the free carrier density  $\Delta N$  is produced, the induced index and absorption for photon frequencies below the semiconductor band gap are given by

$$\begin{aligned} \Delta n &= -\frac{1}{2} \frac{\Delta \tilde{\omega}_p^2}{\omega^2}, \\ \Delta\alpha &= 2 \frac{\Delta n \gamma}{n c}. \end{aligned} \quad (7)$$

The induced absorption that accompanies the change in free-carrier concentration is proportional to the change in refractive index. For GaAs the typical value for the carrier scattering rate is  $\gamma \approx 5 \times 10^{12} \text{ s}^{-1}$ . A change in the free carrier concentration by  $1 \times 10^{18} \text{ cm}^{-3}$  produces an index change of  $\Delta n = 0.002$  and an absorption change of  $\Delta\alpha = 0.6 \text{ cm}^{-1}$ .

### D. Diffraction efficiency

The diffraction efficiency from the combined index and absorption gratings described above is given by<sup>12</sup>

$$\eta = \left[ \sin^2 \left( \frac{\pi \Delta n_K L}{\lambda} \right) + \sinh^2 \left( \frac{\Delta\alpha_K L}{4} \right) \right] \exp[-\alpha(\lambda)L] \quad (8)$$

including absorption, where  $\lambda$  is the free-space wavelength, and  $\Delta n_K$  and  $\Delta\alpha_K$  are the Fourier amplitudes of the refractive index and absorption gratings. This represents an incoherent sum of the contributions to the diffraction efficiency from both the index and the absorption gratings.

## III. THE CHARGE BALANCE APPROXIMATION AND METASTABLE DEFECTS

### A. Charge balance approximation

During optical illumination of a semiconductor with multiple defect levels a dynamic steady state is developed in which quasi-Fermi levels can be assigned to each band edge and to each defect level within the band gap. Because optical illumination places the semiconductor in thermal nonequilibrium, there is no single Fermi level that can be defined for the material. Rigorously, this is also the case when metastable defects are present in the semiconductor. Many of the defects are optically transformed into their metastable states, which represents a highly nonequilibrium condition. Even when the illumination is removed, these defects remain in the metastable states for a long time.

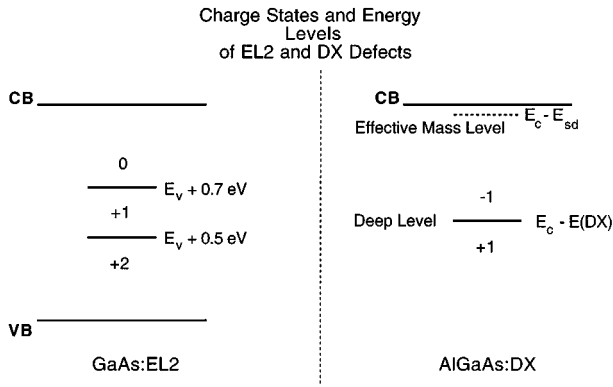


FIG. 1. The energy levels for EL2 in GaAs and DX defect levels in alloys. The energy of the deep DX level depends on alloy composition.

Metastable defects at low temperatures can have lifetimes that are significantly longer than the carrier generation and trapping times of the remaining defects in their normal states. Therefore, when illumination is removed or is very weak, and all carrier generation and capture rates are much larger than the metastable defect regeneration rate, a single nonequilibrium Fermi level can approximately describe the state occupancies of the normal states. In other words, the charge balance between the remaining states in the material behaves as if the metastable states are in permanent stable states. This approximation is called the charge balance approximation (CBA). The value of the CBA is that it can be extended to encompass the case of nonhomogeneous illumination, in which the unique Fermi level becomes a function of position and determines the amount of charge transfer and band bending that occurs for a given exposure. The CBA is expected to break down when the thermal regeneration rate of the metastable defect becomes comparable to the carrier generation and trapping rates of the normal-state defects. The approximation should also break down under intense illumination, during which the normal-to-metastable transformation rate becomes comparable to carrier generation and trapping rates. Therefore, the CBA is appropriate for low temperatures and weak illumination, which are conditions that can be achieved experimentally.

## B. GaAs:EL2

The metastable properties of the defect labeled EL2 in GaAs have been well documented.<sup>13</sup> This defect is considered to be an isolated arsenic antisite, expressed as  $\text{As}_{\text{Ga}}$ , although the possibility that the defect includes a near-neighbor component has been persistent in the literature.<sup>14</sup> The normal-state energy levels are illustrated in Fig. 1. The EL2 defect is a double donor,<sup>15</sup> with energy levels at  $E^{0/+} = E_v + 0.7 \text{ eV}$  and  $E^{+/++} = E_v + 0.5 \text{ eV}$ . Compensation of shallow acceptors by the EL2 defects is the primary source of semi-insulating GaAs substrates, necessary for many integrated circuit applications. Because EL2 is a double donor, it can pin the Fermi level at two different energies within the band gap. When  $N_{\text{EL2}} > (N_{\text{sa}} - N_{\text{sd}})$  then the Fermi level is pinned at an energy near the middle of the band gap, which is the situation in most semi-insulating LEC

GaAs. On the other hand, when  $(N_{\text{sa}} - N_{\text{sd}}) > N_{\text{EL2}} > 0.5(N_{\text{sa}} - N_{\text{sd}})$ , then the Fermi level is pinned at an energy near the second donor level.

The metastable state of the EL2 defect is an excited state of the neutral charge state EL2(0). A photon with a wavelength near  $1.06 \mu\text{m}$  (one of the YAG:Nd laser wavelengths) promotes an electron from the defect ground state to a degenerate excited state.<sup>16</sup> The excited state experiences large lattice relaxation which drives the total energy of the charge state (electronic+elastic energy) to a new energy minimum. At temperatures below 140 K, there is insufficient thermal energy to promote the defect out of the metastable state and back to the normal state. While in this metastable configuration, the defect, though neutral, cannot participate in hole capture because the electronic energy lies outside the band gap.<sup>17-20</sup> Because the metastable state is prevented from participating in charge transfer or compensation mechanisms, the defect has effectively been removed from the material. A new Fermi level will therefore be established which describes the charge balance between the normal-state defects.

When the Fermi level is pinned near the  $E^{0/+}$  midgap level, there is a partial occupancy of both charge states. The neutral charge state EL2(0) is subject to metastable transformation, but the charged state EL2(+) is not. This would appear to disqualify the charged defects from being removed by optical absorption. However, the cross section for photoionization of holes from the EL2(+) defects is nonzero, changing an EL2(+) into an EL2(0) with the liberation of a single hole. The transformed EL2(0) defect is now available for promotion to the metastable state. In this manner, all the photoquenchable EL2 defects can eventually be transformed into the metastable state, regardless of the initial position of the Fermi level. Because holes are liberated during the overall process, the Fermi level shifts from midgap energies to energies near the acceptor level at  $E_{\text{sa}} = E_v + 0.04 \text{ eV}$ .

The exposure needed to transform the EL2 defects into their metastable state is determined by the optical cross sections for electrons and holes as well as by the initial compensation. The defect density is altered by optical illumination by

$$\begin{aligned} N^{\text{EL2}} &= N_0^{\text{EL2}} \exp(-I_0 s^* t) \\ &= N^{\text{EL2}(0)} + N^{\text{EL2}(+)} + N^{\text{EL2}(++)}, \end{aligned} \quad (9)$$

where  $N^{\text{EL2}}$  is the total concentration of normal-state EL2 defects,  $N_0^{\text{EL2}}$  is the initial concentration of all photoquenchable EL2 defects,  $N^{\text{EL2}(i)}$  are the three normal-state charge states, and  $s^*$  is the effective optical cross section for promotion of the EL2 defects to the excited state. The time constant for quenching is

$$\tau = 1/s^* I_0. \quad (10)$$

The effective cross-section  $s^*$  depends in a complicated way on the details of the degree of compensation,<sup>21</sup> which changes in time during illumination. For our purposes in this article, we consider only a simple exponential behavior.

The CBA defines a unique nonequilibrium Fermi level, which determines the densities of the three different charge states, treating the three charge states as permanently stable defects levels. For EL2 this is defined by

$$0 = \frac{N^{\text{EL2}}}{1 + \frac{1}{g} \exp[(E_F - E^{\text{EL2}(0^+)})/k_B T]} + 2 \frac{N^{\text{EL2}}}{1 + \frac{1}{g} \exp[(E_F - E^{\text{EL2}(+/++)})/k_B T]} + N_v \exp[(E_v(x) - E_F)/k_B T] + N_{\text{sd}} - N_{\text{sa}}, \quad (11)$$

where  $N_{\text{sd}}$  and  $N_{\text{sa}}$  are the residual shallow donor and acceptor concentrations and  $g$  is the defect degeneracy. The photoquenched EL2(0)\* defects do not participate in charge compensation, and therefore do not appear in the balance equation. Equation (11) is exact under equilibrium conditions, and is simply the statement of charge neutrality. However, it continues to apply approximately in the case of photoquenched defects at sufficiently low temperatures that normal-state regeneration is negligible.

When the illumination is inhomogeneous the defect concentrations become position dependent through the intensity  $I(x)$  from Eq. (1),

$$N^{\text{EL2}(x)} = N_0^{\text{EL2}} \exp\left(-\frac{t}{\tau} (1 + m \cos Kx)\right). \quad (12)$$

For the discussion of optically induced Fermi level modulation, which is the focus of this article, all properties of the material during illumination will be expressed as functions of exposure, which is measured as a function of time, expressed in units of  $\tau$ .

The photoquenching process converts semi-insulating material into  $p$ -type material. If the illumination is spatially nonuniform, then significant band bending will result from the formation of  $p$ - $i$ - $p$  junctions. During holography, this band bending is the source of large internal electric fields that produce photorefractive gratings. Before performing accurate calculations it is possible to estimate the magnitude of the space-charge fields that are produced by the optically induced Fermi level modulation. The field is given approximately for a sinusoidal peak-to-peak modulation of  $\Delta E_F$  by<sup>3</sup>

$$E_{\text{sc}} = \frac{1}{2} K \Delta E_F. \quad (13)$$

Equation (13) is similar to Eq. (2), but with  $\Delta E_F/2$  exchanged for  $k_B T$ . For a fringe spacing  $\Lambda = 1 \mu\text{m}$  in GaAs and a Fermi level modulation  $\Delta E_F = 0.7 \text{ V}$  the maximum field is  $E_{\text{sc}} = 22 \text{ kV/cm}$ , which produces an index change  $\Delta n = 5 \times 10^{-5}$ . Accurate numerical calculations are presented in the following sections which substantiate this estimate. It is also important that the optically induced Fermi level modulation in the crystal is not sinusoidal, and it is only the first spatial Fourier coefficient that is important for diffraction according to Eq. (8).

## C. DX centers

The so-called DX defects<sup>22</sup> are a class of defects that occur in most III–V and II–VI semiconductors that are doped  $n$  type and that have alloy compositions that place them in or near the range of indirect band gaps. This class of defect has been thoroughly studied<sup>2</sup> because of their technological impact for devices operating at low temperatures. The principle signature of the DX defects is persistent photoconductivity after illumination of the crystals at temperatures below 100 K. The persistent photoconductivity is caused by a defect metastability. There was considerable debate concerning the origin of the metastability,<sup>22</sup> but it is now widely accepted that the DX defects are substitutional donor dopant atoms that undergo large lattice relaxation after photoexcitation.<sup>18</sup> An additional peculiarity of the DX defects is that they behave as negative-U defects,<sup>23</sup> in which the defect occurs in a negative DX(–) charge state with no stable neutral charge state. During the photoemission of one electron, the defect spontaneously emits a second electron. Conversely, the transformation from the metastable state to the normal state requires the capture of two electrons. The energy levels of the DX defect are shown in Fig. 1. The DX(–) state is the thermodynamically stable state. When the defect is in the metastable DX\* state it appears as an effective mass level tied to the conduction band minimum.

The location of the Fermi level in these  $n$ -doped materials is determined by a self-compensation mechanism. Because of the negative-U behavior of the DX defects, and because of the typically high  $n$ -type doping levels, the equilibrium Fermi level is set by a balance between the effective mass level and the DX(–) defects, in which approximately half of the donor atoms donate their electrons to the stable DX(–) states. When no other defects are present in the material, the initial defect concentrations are approximately

$$N_0^{\text{DX}} = N_0^{\text{DX}*} = \frac{1}{2} N_D,$$

where  $N_D$  is the density of donor atoms. Under optical illumination the concentrations of the normal-state and metastable defects evolve with optical exposure as

$$N^{\text{DX}} = N_0^{\text{DX}} \exp\left(-\frac{t}{\tau}\right),$$

$$N^{\text{DX}*} = N_0^{\text{DX}*} + N_0^{\text{DX}} \left[1 - \exp\left(-\frac{t}{\tau}\right)\right],$$

where  $N_0^{\text{DX}}$  is the initial concentration of normal-state DX defects,  $N_0^{\text{DX}*}$  is the initial concentration of metastable DX defect states, and  $t$  is the exposure time.

The CBA is used to define a unique Fermi level after partial illumination. The CBA for the DX defects is substantially different than for the case of GaAs:EL2, in which the optical transformation to the metastable EL2\* state prevents that defect state from compensating shallow acceptors. The CBA treats both the DX(–) and effective mass states as distinct stable (permanent) defect states with separate energy levels within the band gap. The charge neutrality condition that sets the unique Fermi level is therefore given by

$$0 = \frac{N^{\text{DX}*}}{1 + \frac{1}{g^*} \exp[(E_F - E^{\text{DX}*})/k_B T]} - \frac{N^{\text{DX}}}{1 + \frac{1}{g} \exp[(E_F - E^{\text{DX}})/k_B T]} - \frac{1}{2\pi^2} \left( \frac{2m^*}{\hbar^2} \right)^{3/2} \int_{-\infty}^{\infty} \frac{(\epsilon - E_c)^{1/2}}{1 + \exp[(\epsilon - E_F)/k_B T]} d\epsilon, \quad (14)$$

where the degenerate expression for the conduction band is used and the hole concentration in the valence band has been neglected.

At low temperature the Fermi level is pinned between the DX level and the DX\* level. With increasing partial illumination the CBA positions the Fermi level increasingly higher in the band gap, until sufficient photocarriers have been excited to move the Fermi level inside the conduction band, making the semiconductor degenerate. Under spatially inhomogeneous partial illumination, the DX and DX\* densities evolve according to

$$N^{\text{DX}}(x) = N_0^{\text{DX}} \exp\left(-\frac{t}{\tau}(1 + m \cos Kx)\right),$$

$$N^{\text{DX}*}(x) = N_0^{\text{DX}*} + N_0^{\text{DX}} \left[ 1 - \exp\left(-\frac{t}{\tau}(1 + m \cos Kx)\right) \right],$$

where the exposure time  $\tau$  is given by Eq. (10) with appropriate optical cross sections. As before, an estimate of the internal electric fields can be made based on charge transfer from the bright to the dark fringes. In the case of the DX defects Eq. (13) is still valid, but  $\Delta E_F$  is considerably smaller, with a maximum value around 100 meV. For a 1  $\mu\text{m}$  fringe spacing, the space-charge electric field is approximately 3 kV/cm, which is an order-of-magnitude smaller than for the EL2 defects. However the metastable optical gratings based on plasma gratings can be large.

#### IV. ADIABATIC MODULATION DOPING

Modulation doping of semiconductors has previously been reserved for epitaxial growth, in which the defect densities and local compensation are controlled as a function of growth thickness, or by spatially modulated ion implants. Both of these techniques are restricted to thicknesses within several microns. On the other hand, the optically induced metastability of defects introduce a new avenue to produce modulation-doped structures that extend throughout the bulk volume of a crystal.

While the CBA assumes that the thermal regeneration rate is much smaller than transition rates, the adiabatic modulation doping approximation assumes that the photoquenching rate is much smaller than the charge transport rates in the material. The time evolution of the optically induced Fermi-level modulation can therefore be considered as a function of exposure. This adiabatic limit neglects all dy-

namic transport processes, and treats the crystal at successive times as if it were in complete thermal equilibrium with spatially modulated defect concentrations.

Fermi level modulation in the adiabatic limit is described by Poisson's equation,

$$\nabla^2 \phi(x) = -\frac{e}{\epsilon \epsilon_0} \left[ \sum_q q N^q(x) + p(x) - n(x) \right], \quad (15)$$

where  $N^q$  is the density of defects with charge  $q$ , including both deep and shallow defects,  $p(x)$  and  $n(x)$  are the free hole and electron concentrations, and  $\phi(x)$  is the electrostatic potential. All the quantities in Eq. (15) are space dependent, and all must satisfy pseudothermal equilibrium with  $E_F = \text{const}$ . This condition places the following constraints on the space-dependent energies:

$$E_v(x) = -e\phi(x),$$

$$E_c(x) = E_g - e\phi(x), \quad (16)$$

$$E^q(x) = E_0^q - e\phi(x),$$

which control the free-carrier densities

$$n(x) = \frac{1}{2\pi^2} \left( \frac{2m^*}{\hbar^2} \right)^{3/2} \int_{-\infty}^{\infty} \frac{[\epsilon - E_c(x)]^{1/2}}{1 + \exp[(\epsilon - E_F)/k_B T]} d\epsilon,$$

$$p(x) = N_v \exp((E_v(x) - E_F)/k_B T), \quad (17)$$

where the expression for a degenerate electron gas is included explicitly, and which control the defect densities

$$N^q(x) = \frac{N_0^q(x)}{1 + \frac{1}{g_q} \exp[(E_F - E^q(x))/k_B T]}. \quad (18)$$

These equations contribute to Eq. (15), which is solved with periodic boundary conditions.

#### V. OPTICALLY INDUCED FERMI-LEVEL MODULATION IN GaAs:EL2

The band and defect energies for a near-optimal exposure are illustrated in Fig. 2 for a single fringe period. In this case the band bending is calculated to respond to a sinusoidal intensity pattern. The EL2 defects have been nearly completely photoquenched in the bright fringe, and the Fermi level has dropped to near the valence band maximum. However, in the center of the dark fringe the Fermi level remains pinned at the midgap EL2 level. The band bending is produced by charge transfer from the bright to the dark fringe. During the photoquenching process, holes are liberated from the EL2 defect level. There are insufficient acceptor levels in the bright fringe to compensate this charge, forcing the holes to migrate to the dark fringes, where they are trapped at the normal-state EL2 defects still present there. This macroscopic charge transfer forms a  $p$ - $i$ - $p$ - $i$  modulation doped structure. The electric fields between the bright and dark fringes can be large in this case, approaching magnitudes of 20 kV/cm, producing refractive index changes of  $\Delta n = 10^{-4}$ .

The valence band energy across a single fringe is shown in Fig. 3 as a function of the logarithm of the exposure. The parameters chosen for the simulation are  $N_{\text{EL2}} = 4 \times 10^{16}$

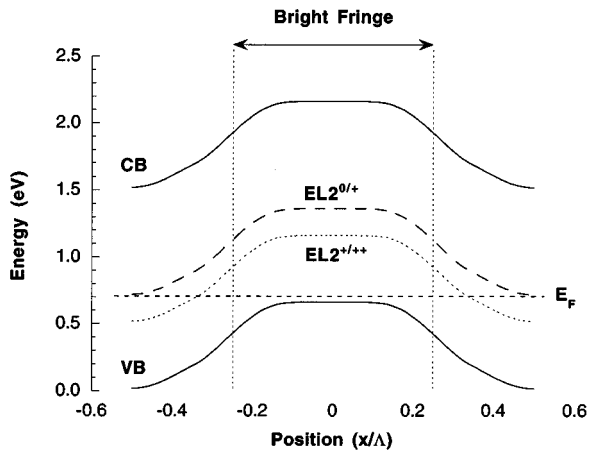


FIG. 2. Band energies of GaAs:EL2 showing the band bending across one fringe period for a near-optimal exposure. The Fermi level remains pinned midgap in the dark fringe, but has moved near the top of the valence band in the bright fringes.

$\text{cm}^{-3}$ ,  $\Lambda = 1 \mu\text{m}$ , and a compensation ratio  $r = 0.7$ , defined as  $r = N_{\text{sa}}/N_{\text{EL2}}$ . Because EL2 is a double donor, the compensation ratio can vary from 0 to 2.0. When  $r > 2.0$ , the shallow acceptors are no longer compensated by the EL2 defects and the material becomes  $p$  type. The Fermi level is constant in Fig. 3 and occurs at the top plane of the figure. At early times the valence band is flat and the Fermi level is pinned midgap by the  $\text{EL2}^{0/+}$  level. For weak exposure, as the neutral EL2 are converted into metastable states, the Fermi level drops to the second ionization level of  $\text{EL2}^{+/++}$  and the valence band moves up by  $\Delta E = E(\text{EL2}^{0/+}) - E(\text{EL2}^{+/++})$  in the bright fringe. For increasing exposure, the final EL2 defects in the bright fringe are quenched, and the Fermi level drops to the top of the valence band. The valence band energy in Fig. 3 therefore rises in the bright fringe by an additional  $\Delta E = E(\text{EL2}^{+/++}) - E_v$ . For even later times, the Fermi level

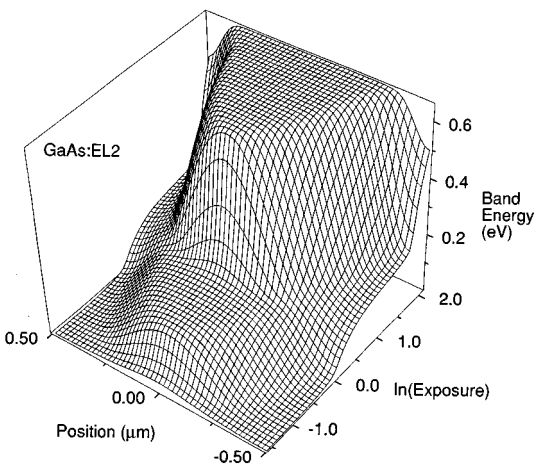


FIG. 3. The EL2 band energy surface across one fringe period as a function of exposure for  $m = 0.9$ ,  $N_{\text{EL2}} = 4 \times 10^{16} \text{cm}^{-3}$ , and  $r = 0.7$ . The bright fringe is in the center. The Fermi level is constant across the top of the cube. The steps in the band bending from the first and second ionization levels of EL2 are seen with increasing exposure.

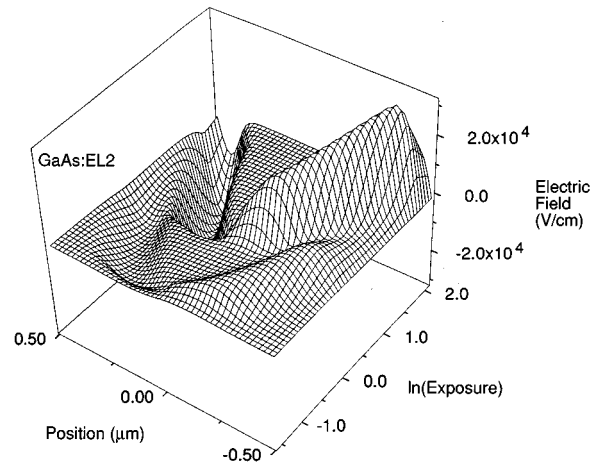


FIG. 4. The space-charge electric field for the conditions of Fig. 3. The peak local field magnitude approaches 20 kV/cm. The contributions from the two ionization levels are clearly seen.

drops everywhere to the top of the valence band as the EL2 defects in the dark fringe are quenched, and flatband conditions are achieved again, but now as uniform  $p$ -type material.

The internal space-charge electric field for these same conditions is shown in Fig. 4 as a function of the natural logarithm of the exposure. The field amplitude approaches 20 kV/cm for late times for maximum Fermi level modulation. Structure from both the  $\text{EL2}^{0/+}$  level as well as the  $\text{EL2}^{+/++}$  level are present as the Fermi level pins at the first, then the second energy level. For moderately late times (moderate exposures) full modulation of the Fermi level across half the band gap is established. It is important to point out that the induced index changes, caused by the non-uniform illumination, are nonlocal to the optical stimulus. This feature is similar to the traditional photorefractive effect operating under diffusion. The migration of charge from the bright fringe to the dark fringe produces a maximum electric field that is shifted by a quarter fringe spacing relative to the intensity maximum. The nonlocal nature of photorefractive nonlinear optics has important consequences for the interaction of multiple coherent laser fields, including two-wave mixing gain and self-pumped phase conjugation.<sup>24</sup> These phenomena should also be relevant to the metastable gratings described here.

Diffraction from the index gratings induced by the electric fields depends only on the first spatial Fourier coefficient of the electric field. Therefore, the peak magnitude of the field does not give a direct measure of the diffracted signal as a function of exposure. The first spatial Fourier coefficient of the induced refractive index grating is shown in Fig. 5 as a function of exposure for a fringe spacing of  $1 \mu\text{m}$  and a compensation ratio  $r = 1.0$ . The general features in Fig. 5 match qualitatively with experimental results,<sup>3</sup> which show a fast rise and a slower decay. However, the change in the slope of the decay that arises from the temporary pinning of the Fermi level at the second ionization level of EL2 has not been observed experimentally. The magnitudes shown in Fig. 5 also have not been observed experimentally, indicat-

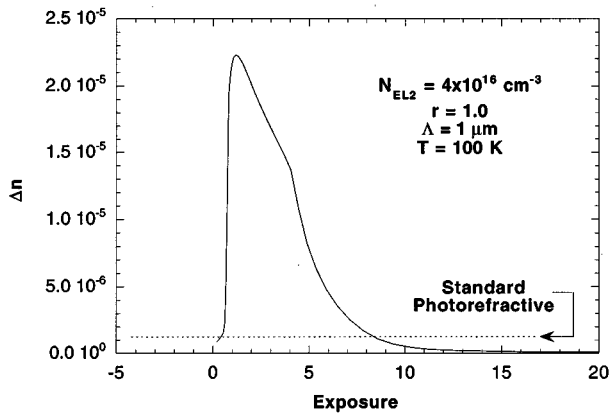


FIG. 5. First spatial Fourier coefficient of the refractive index grating as a function of exposure for  $m=0.9$ ,  $N_{EL2}=4\times 10^{16} \text{ cm}^{-3}$ ,  $\Lambda=1 \mu\text{m}$ , and  $r=1.0$ . The fast rise and slow decay of the diffracted signal is in qualitative agreement with experiment (Ref. 4).

ing that full Fermi-level modulation has not been achieved in the experiments.<sup>6</sup> One likely cause of the lack of full modulation would be additional deep defect levels that prevent the Fermi level from shifting to the top of the valence band.

Optically induced Fermi-level modulation is sensitive to the initial compensation between the deep EL2 defects and the shallow acceptors. Especially when the compensation ratio falls below  $r=1.0$ , the Fermi level is not strongly pinned at the midgap EL2 level. Also, the maximum allowable charge transfer that generates the band bending becomes limited by lack of available defects to trap and store space charge, causing the gratings to be trap limited at short fringe spacings.

The first spatial Fourier coefficient of the induced refractive index grating is shown in Fig. 6 as a function of fringe spacing for several compensation ratios for an EL2 concentration of  $4\times 10^{16} \text{ cm}^{-3}$  and an exposure of  $\tau=1$ . The index change from the diffusion field in Eqs. (2) and (3) at  $T=100 \text{ K}$  is shown for comparison. For small compensation ratios the optically induced Fermi level modulation is severely limited by lack of available sites to trap and store space charge.

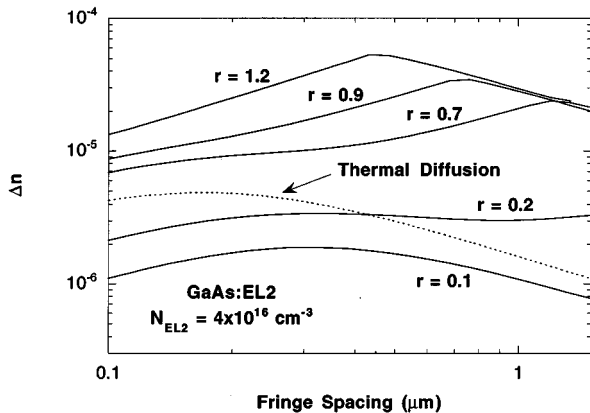


FIG. 6. First spatial Fourier coefficient of the refractive index grating as a function of fringe spacing for a family of compensation ratios for  $N_{EL2}=4\times 10^{16} \text{ cm}^{-3}$ . Weak compensation severely limits the available defect sites for charge transfer.

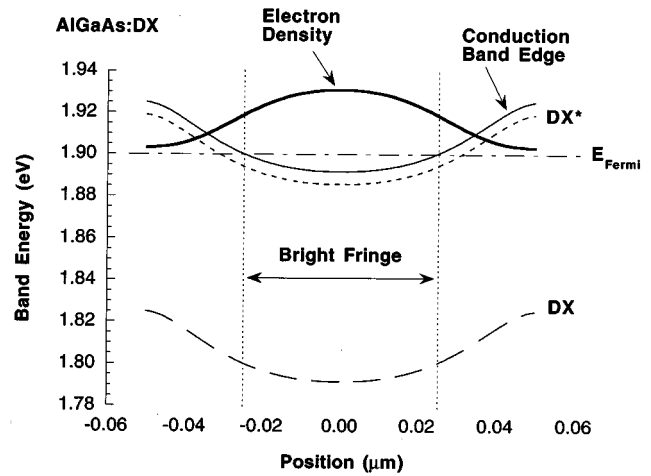


FIG. 7. Band bending and electron density for AlGaAs:DX. The binding energy of the stable DX state is at  $E_c-100 \text{ meV}$ . Moderate band bending occurs, with a peak-to-peak modulation of approximately 40 meV. The Fermi level is degenerate in the bright fringe, and the electron density is shown for comparison.

In this extreme case the index change from a traditional diffusion field can be larger than from the optically induced Fermi-level modulation. On the other hand, for compensation ratios close to  $r=1.0$ , the optically induced Fermi-level modulation can exceed the traditional diffusion field by over one order of magnitude. Even in this case, the Fermi-level modulation becomes trap limited for fringe spacings smaller than approximately  $0.5 \mu\text{m}$ . It is important to note that larger initial EL2 concentrations will support shorter fringe spacings, but as-grown EL2 concentrations from bulk LEC GaAs are typically limited to concentrations below  $10^{17} \text{ cm}^{-3}$ . Much larger EL2 densities may be achievable using low-temperature growth during molecular beam epitaxy.<sup>25</sup>

## VI. FREE-CARRIER PLASMA GRATINGS FROM DX CENTERS

The band bending and electron density across one fringe spacing for AlGaAs:DX is illustrated in Fig. 7. In the figure the stable DX level has a binding energy of 100 meV, and the metastable DX\* level is an effective mass level below the direct conduction band edge. In the bright fringe, the optical illumination liberates electrons from the DX defects into the conduction band. The material remains approximately locally neutral, with the electrons bound to the metastable DX\* defects. However, the optical modulation of the DX density produces a moderate band bending with a peak-to-valley amplitude of approximately 40 meV. The band bending is associated with macroscopic charge transfer and the buildup of space-charge fields, which represents a moderate deviation from strict local charge neutrality.

The free carrier density is shown as a function of exposure across one fringe spacing in Fig. 8 for a DX density of  $1\times 10^{18} \text{ cm}^{-3}$ , with the dark fringe centered in the figure. At the optimal exposure a free carrier density of  $3\times 10^{17} \text{ cm}^{-3}$  is generated with a peak-to-valley amplitude of  $2\times 10^{17} \text{ cm}^{-3}$ . This free-carrier modulation produces an index change from Eq. (7) of  $\Delta n=10^{-4}$ , calculated for a probe-beam wave-

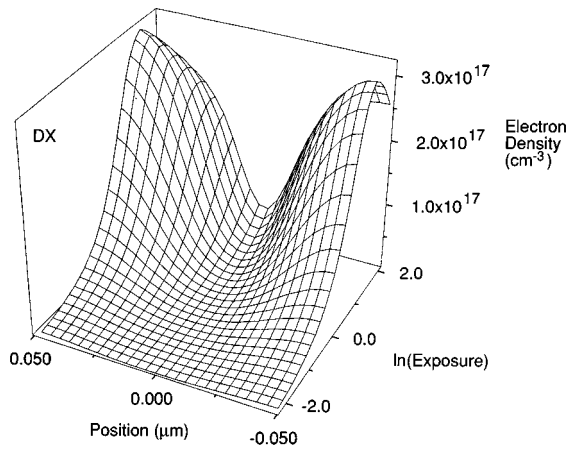


FIG. 8. Free carrier density as a function of exposure across one fringe spacing for a donor concentration of  $1 \times 10^{18} \text{ cm}^{-3}$  and a fringe spacing of  $0.1 \mu\text{m}$ . A peak electron density of  $3 \times 10^{17} \text{ cm}^{-3}$  is generated in this case. The dark fringe is at the center.

length of  $1.5 \mu\text{m}$ . For long exposures the free carrier density becomes uniformly distributed and the grating amplitude decreases. The space-charge electric field associated with the Fermi-level modulation is shown in Fig. 9 for the same conditions as Fig. 8. The electric field reaches a maximum value of  $10 \text{ kV/cm}$ , which produces an index change of  $\Delta n = 2 \times 10^{-5}$  for a holographic-cut crystal. As in the case of GaAs:EL2 and the traditional photorefractive effect, this electric field produces a nonlocal index change, with the associated consequences.<sup>24</sup> However, the plasma gratings are considerably larger than the Fermi-level modulation gratings. The evolution of the respective index gratings as functions of exposure are shown in Fig. 10. The Fermi-level grating is larger than the plasma grating at low exposure, but the plasma grating rapidly becomes the strongest grating in the material.

An important issue for holographic information storage is the minimum possible fringe spacing that can be supported during holographic writing. The extremely high doping levels that are possible for DX defects suggests that extremely

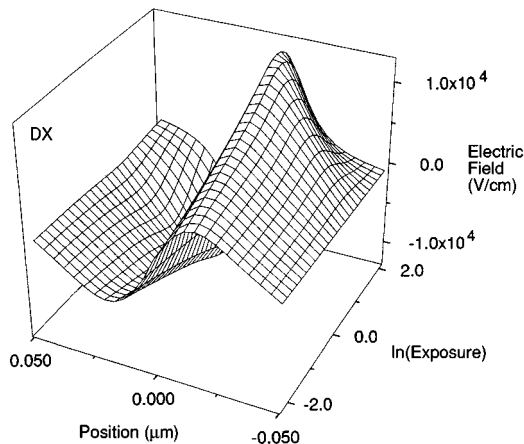


FIG. 9. Space-charge electric field associated with the band bending of Fig. 8. A peak field of  $10 \text{ kV/cm}$  is produced.

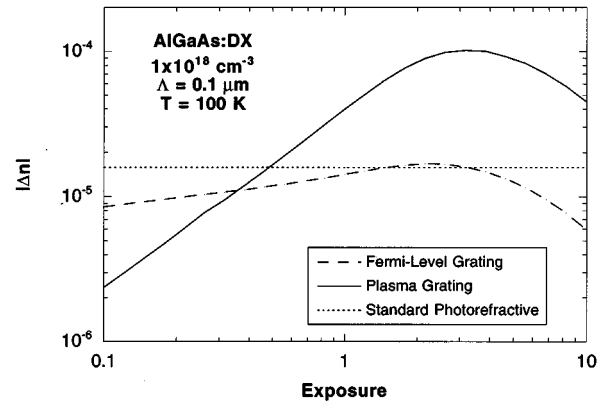


FIG. 10. Index changes from the plasma grating and from the Fermi level modulation as functions of exposure in a holographic-cut crystal for a donor concentration of  $1 \times 10^{18} \text{ cm}^{-3}$  and a fringe spacing of  $0.1 \mu\text{m}$ . The standard photorefractive diffusion-field case is shown for comparison. The Fermi-level modulation gratings are overtaken by the plasma grating for higher exposures.

fine spatial resolution should be possible. While the assumption of local charge neutrality<sup>9</sup> is a good approximation at large fringe spacings, it must fail at short fringe spacings because of the charge transfer from Fermi-level modulation. This is illustrated in Fig. 11 for the Fermi-level gratings and the plasma gratings as functions of fringe spacing for extremely short fringe spacings. The rapid decrease of the plasma grating with decreasing fringe spacing coincides with the onset of trap limitation for the Fermi-level gratings. This occurs for fringe spacings of approximately  $400 \text{ \AA}$ . It is important to note that the Thomas-Fermi screening length for this electron density is approximately  $60 \text{ \AA}$ , which is an order-of-magnitude smaller than the cut-off seen in Fig. 11. Therefore, the limit of spatial resolution for plasma gratings is set by Fermi-level modulation, rather than by Thomas-Fermi screening, even though the semiconductor is degenerate.

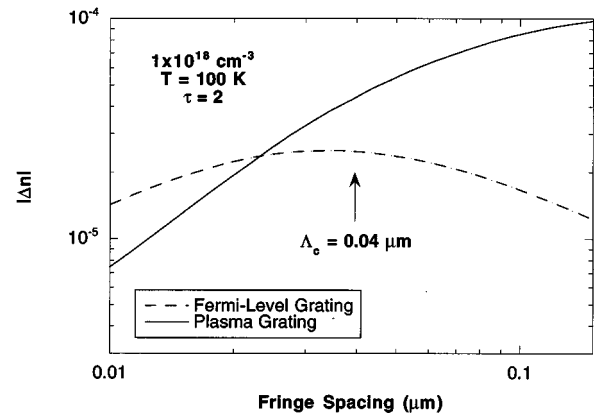


FIG. 11. Comparison of the fringe spacing dependencies of the plasma gratings and the Fermi-level modulation gratings. The rapid decrease of the plasma gratings with decreasing fringe spacing below  $0.04 \mu\text{m}$  coincides with the onset of trap limitation of the Fermi-level gratings.

## VII. CONCLUDING REMARKS

The metastable optical gratings described here share much in common with photorefractive effects, but have the advantage of integration of illumination with near-unity quantum efficiency without relaxation. Furthermore, the size of the optical changes are not limited by steady-state conditions, such as the diffusion field of Eq. (2). However, there are factors that limit the usefulness of these metastable gratings for holographic optical memory. The first practical limitation is due to defect complexes that impede the transition to the metastable state. It is well known that not all arsenic-antisite-related defects are photoquenchable.<sup>13</sup> High defect concentrations that cause defect pairs can limit the quantum efficiency for generating the grating, or can cause trap limitation for charge transfer. A more serious problem, especially for the case of GaAs:EL2, is the presence of additional defect levels within the band gap due to uncontrolled impurities. The Fermi level may be pinned at these additional levels, preventing a full modulation of the Fermi level. The diffraction efficiencies observed experimentally are limited by such additional impurity levels. These limiting effects due to unwanted defects can in principle be removed by more careful control of the incorporation of impurities during crystal growth.

The second and more fundamental limitation is the persistence of the metastable gratings only for temperatures below 150 K. For practical and widespread application, room temperature operation is necessary. The physical parameter that limits this effect to low temperatures is the regeneration energy barrier for regeneration from the metastable to the stable state. For EL2 the regeneration energy is 300 meV and for DX-related defects the energy is around 200 meV for both III-V and II-VI semiconductors. On the other hand regeneration energies in excess of 400 meV would be necessary for room-temperature operation. It is not currently known whether this large regeneration barrier can be achieved for any metastable defects in the traditional semiconductors. However, there is variability in the regeneration energy values, and it may be possible to discover trends that would allow the regeneration energy to be maximized. It will also be important to explore defect metastabilities in unconventional semiconductors<sup>26</sup> or in oxides where regeneration energies could be larger than in the covalent semiconductors.

Theoretical extensions of the work presented here should address two additional aspects that can arise during experiments. The first is the aspect of intermediate temperatures for which the thermal regeneration rate from the metastable to normal defect states becomes non-negligible. Under this con-

dition, the simple charge balance approximation described by Eqs. (11) and (14) will need to be extended and will become a function of optical intensity. The second extension is the inclusion of time-dependent effects and the dynamic evolution of the metastable gratings. Under high-intensity illumination the adiabatic modulation doping approximation will break down because the quenching rates will become comparable to charge transport rates. Each of these extensions, in addition to including the role of multiple defect levels, should provide an accurate theoretical match to experimental results on metastable optical gratings in semiconductors.

<sup>1</sup>S. T. Pantelides, *Deep Centers in Semiconductors* (Gordon and Breach, New York, 1986).

<sup>2</sup>P. M. Mooney, *J. Appl. Phys.* **67**, R1 (1990).

<sup>3</sup>D. D. Nolte, D. H. Olson, and A. M. Glass, *Phys. Rev. B* **40**, 10 650 (1989).

<sup>4</sup>D. D. Nolte and R. S. Rana, in *Proceedings of the 20th International Conference on Physical Semiconductors* (World Scientific, Singapore, 1990), p. 2247.

<sup>5</sup>P. Delaye and B. Sugg, *Phys. Rev. B* **50**, 16 973 (1994).

<sup>6</sup>R. S. Rana, thesis, Purdue University, 1996.

<sup>7</sup>R. A. Linke, T. Thio, J. Chadi, and G. E. Devlin, *Appl. Phys. Lett.* **65**, 16 (1994).

<sup>8</sup>R. L. MacDonald, R. A. Linke, J. D. Chadi, T. Thio, G. E. Devlin, and P. Becla, *Appl. Phys. Lett.* **19**, 2131 (1994).

<sup>9</sup>R. L. MacDonald, R. A. Linke, G. E. Devlin, and M. Mizuta (unpublished).

<sup>10</sup>D. D. Nolte, in *Photorefractive Effects and Materials*, edited by D. D. Nolte (Kluwer, Dordrecht, 1995).

<sup>11</sup>C. Kittel, *Introduction to Solid State Physics* (Wiley, New York, 1986).

<sup>12</sup>H. Kogelnik, *Bell Sys. Tech. J.* **48**, 2909 (1969).

<sup>13</sup>G. M. Martin and S. Makram-Ebeid, in *Deep Centers in Semiconductors*, edited by S. T. Pantelides (Gordon and Breach, New York, 1985).

<sup>14</sup>J. M. Spaeth, in *Proceedings of 4th International Conference on Semiconducting III-V Materials*, 1986.

<sup>15</sup>J. Lagowski, D. G. Lin, T. Chen, M. Skowronski, and H. C. Gatos, *Appl. Phys. Lett.* **47**, 929 (1985).

<sup>16</sup>M. Kaminska, M. Skowronski, J. Iagowski, J. M. Parsey, and H. C. Gatos, *Appl. Phys. Lett.* **43**, 302 (1983).

<sup>17</sup>D. J. Chadi and K. J. Chang, *Phys. Rev. Lett.* **60**, 2187 (1988).

<sup>18</sup>D. J. Chadi and K. J. Chang, *Phys. Rev. B* **39**, 10 063 (1989).

<sup>19</sup>J. Dabrowski and M. Scheffler, *Phys. Rev. B* **40**, 10 391 (1989).

<sup>20</sup>J. Dabrowski and M. Scheffler, *Phys. Rev. B* **60**, 2183 (1988).

<sup>21</sup>G. Vincent, D. Bois, and A. Chantre, *J. Appl. Phys.* **53**, 3643 (1982).

<sup>22</sup>D. V. Lang and R. A. Logan, *Phys. Rev. B* **19**, 1015 (1979).

<sup>23</sup>D. J. Chadi and K. J. Chang, *Phys. Rev. Lett.* **61**, 873 (1988).

<sup>24</sup>P. Günter and J.-P. Huignard, *Photorefractive Materials and Their Applications I and II*, Topics in Applied Physics Vol. 16 (Springer, Berlin, 1988).

<sup>25</sup>D. C. Look, D. C. Walters, M. Nier, C. E. Stutz, and S. K. Brierley, *Appl. Phys. Lett.* **60**, 2900 (1992).

<sup>26</sup>A. I. Ryskin, A. S. Shcheulin, B. Koziarska, J. M. Langer, A. Suchocki, I. I. Buczinskaya, P. P. Fedorov, and B. P. Sobolev, *Appl. Phys. Lett.* **67**, 31 (1995).